

# Real time Quantum state holography using coherent transients

Antoine Monmayrant, Béatrice Chatel, and Bertrand Girard

*Laboratoire Collisions, Agrégats, Réactivité (UMR 5589 CNRS-UPS),*

*IRSAMC, Université Paul Sabatier Toulouse 3, 31062 Toulouse cedex 9, France*

(Dated: 30 janvier 2006)

In a two level atom, real-time quantum state holography is performed through interferences between quantum states created by a reference pulse and a chirped pulse resulting in coherent transients. A sequence of several measurements allows one to measure the real and imaginary parts of the excited state wave function. These measurements are performed during the interaction with the ultrashort laser pulse. The extreme sensitivity of this method to the pulse shape provides a tool for electric field measurement.

## I. INTRODUCTION

The effect of laser pulse shape on a quantum system is related to the nature of the interaction. For a linear response of the system (one-photon transition in the weak field regime), the final outcome depends only on the spectral component at the resonance frequency and is therefore independent of the pulse shape, and particularly of the spectral phase [1]. This explains for instance why signals equivalent to wave-packet interferences could be observed with incoherent light as well as with ultrashort pulses [2]. However, the temporal evolution towards the final state may depend strongly on the pulse shape. A straightforward illustration of this statement is the non-resonant interaction which leads to transient excitation of the system, but to no final excitation. In the absence of predesigned control mechanisms only a closed loop scheme [3, 4] may be employed to find efficient pulse shapes [5, 6, 7, 8] : The outcome of many different shapes is fed back into an algorithm that iteratively optimizes the excitation shape without insight into the physical mechanism that is triggered by a particular shape.

In contrast the effect of shapes on small systems can be systematically studied within an open-loop scheme [9, 10, 11, 12]. This open-loop approach is well adapted to these systems for which theoretical predictions are reliable. It consists of reaching a specific goal (manipulation

of the temporal response of a system excited by a light pulse) without any experimental feedback. Physical analysis of the process allows one to predetermine the theoretical pulse shape which leads to the desired result. It is then implemented experimentally.

In this article, we describe manipulation of Coherent Transients (CT) in an open loop approach. These CT are oscillations in the excited state population resulting from the interaction between a two-level system and a weak chirped pulse. The shape of these oscillations is extremely sensitive to slight changes in the pulse shape [12, 13]. Two previous letters [14, 15] have shown that their high sensitivity provides a new scheme for quantum state measurement and electric field reconstruction. This article presents in details the works and calculations corresponding to these results. First we recall the coherent transients and how to manipulate them. Then the quantum state measurement reconstruction is presented in detail. In particular several schemes are discussed. Then the experimental set-up and several previous feasibility test are described. Finally the results are presented and discussed.

## II. COHERENT TRANSIENTS PRINCIPLE

The CT result from the interaction of a two-level system ( $|g\rangle$  and  $|e\rangle$ ) with a chirped pulse  $E_{pu}(t)$  of carrier angular frequency  $\omega_{pu}$  close to resonance ( $\omega_{pu} \simeq \omega_{eg}$ ). The transient excited state population is probed towards the  $|f\rangle$  level in real time by a second ultrashort pulse  $E_{pr}(t)$  which is Fourier transform limited and short compared to the characteristic features of  $E_{pu}(t)$ . Its frequency is close to resonance ( $\omega_{fe}$ ). The fluorescence arising from the  $|f\rangle$  state is then recorded as a function of the pump-probe delay  $\tau$  (cf Fig. 1). The probe

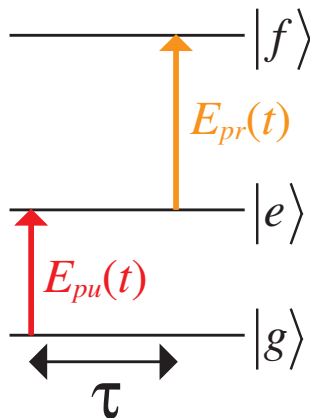


FIG. 1 – Excitation scheme.

pulse provides access to the temporal evolution of the population in  $|e\rangle$ , produced by the pump beam. The result of the interaction is described by first order perturbation theory, and the fluorescence is proportional to

$$S(\tau) = |a_f(\tau)|^2 \propto \left| \int_{-\infty}^{+\infty} E_{pr}(t-\tau) \exp(i\omega_{fe}(t-\tau)) a_e(t) dt \right|^2 \quad (1)$$

with

$$a_e(t) = \int_{-\infty}^t E_{pu}(t') \exp(i\omega_{eg}t') dt' = \int_{-\infty}^t e^{-(t'/\tau_{pu})^2} e^{-i(\delta\omega_{eg}t' + \alpha_{pu}t'^2)} dt' \quad (2)$$

in the case of a simply chirped pulse  $E_{pu}(t) = e^{-(t/\tau_{pu})^2} e^{-i(\omega_{pu}t + \alpha_{pu}t^2)}$ . Here  $\delta\omega_{eg} = \omega_{pu} - \omega_{eg}$  is the resonance mismatch,  $\tau_{pu}$  the pulse duration and  $\alpha_{pu}$  the chirp rate. A quadratic phase appears in the integral giving  $a_e(t)$  (Eq. 2), leading to oscillations of the probability  $|a_f(\tau)|^2$  as already demonstrated [12, 16] (cf Fig. 2). These strong oscillations result from interferences between the probability amplitude excited at resonance and after resonance.

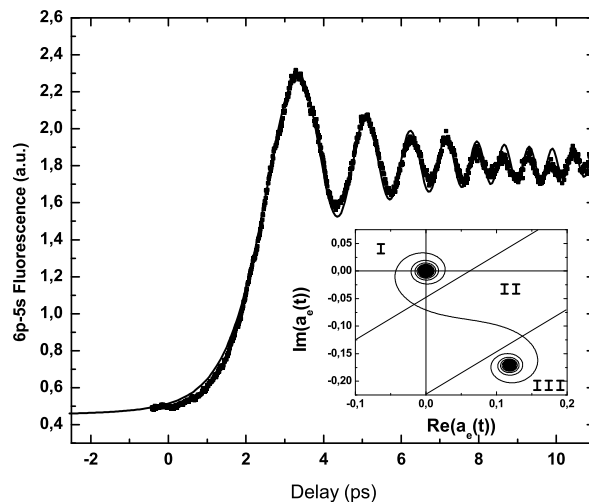


FIG. 2 – Experimental Coherent Transients on Rb ( $5s-5p_{1/2}$  at  $\lambda = 795$  nm), for a chirp of  $-8.10^5$  fs<sup>2</sup> (dots) and the corresponding simulation obtained by numerical resolution of the Schrödinger equation (solid line) [16]. Inset : Theoretical excited state amplitude drawn in the complex plane.

The CT phenomenon is better understood by examining the behavior of  $a_e(t)$  in the complex plane as displayed in the inset of Fig. 2. The probability amplitude follows a Cornu

spiral starting from the origin. Three regions can be distinguished. The two spirals result from contributions before (I) and after (III) resonance for which the quadratic phase varies rapidly. The intermediate region (II) corresponds to the passage through resonance where the phase is stationary. It provides the main contribution to the population. The two spirals, although similar, result in totally different behaviors of the population. The first one (I) winds round the origin with an increasing radius. The resulting probability increases thus slowly and regularly and remains small. After resonance (III), a second spiral winds round the asymptotic value leading to strong oscillations of the population.

We show in the next section how a modification of the excitation scheme provides the possibility to observe oscillations due to the first part of the pulse.

### III. QUANTUM STATE MEASUREMENTS

#### A. principle

The CTs are extremely sensitive to tiny phase modifications of the pump pulse [12, 13]. Therefore, they can provide detailed information on the exciting pulse and simultaneously on the excited quantum state. However, although sensitive to phase effects these CTs give access to the excited state probability  $|a_e(\tau)|^2$  whereas the probability amplitude is necessary to achieve a complete measurement of the electric field. Moreover, the oscillations are only produced by the second part of the pulse (after resonance)[16]. To overcome these limitations, we propose a new excitation scheme based on a two pulse sequence with a well defined phase relationship. The pump pulse is written as

$$E_{pu}(t) = E_{pu_1}(t) + e^{i\theta} E_{pu_2}(t) \quad (3)$$

where  $E_{pu_1}(t)$  and  $E_{pu_2}(t)$  are two replica of the initial pulse with additional spectral phase. These can be obtained with either a Michelson-type interferometer or a pulse shaper. The first pulse  $E_{pu_1}(t)$  creates an initial population in the excited state. The second pulse  $E_{pu_2}(t)$  is strongly chirped and sufficiently delayed so that it does not overlap with the first pulse. This second pulse creates a probability amplitude in the excited state which interferes with the initial probability amplitude created by the first pulse.

It should be noted that the details of the shape of the first pulse are not critical. Only the final state reached at the end of the first pulse is involved in the temporal evolution of

the system during the second pulse.

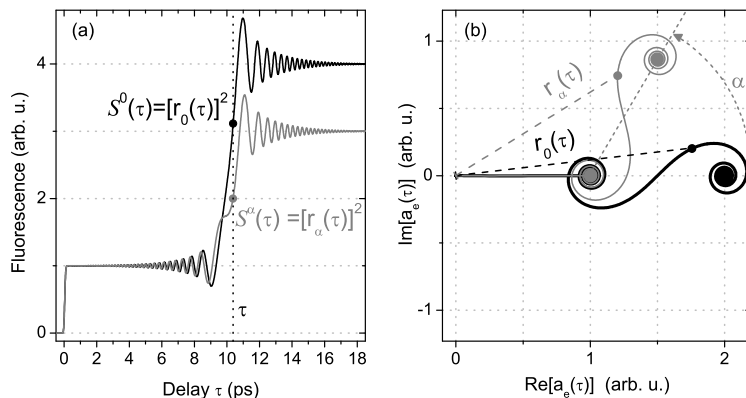


FIG. 3 – (a) Theoretical CTs scans for a geometric reconstruction :  $\theta = 0$  (black),  $\theta = \alpha$  (gray), with  $\phi_{pu}^{(1)} = 10$  ps,  $\phi_{pu}^{(2)} = 2.10^5$  fs<sup>2</sup>. (b) Corresponding probability amplitudes (same color code).

Looking at the evolution of the quantum state in the complex plane (Fig. 3 (b)), one sees that the effect of the first pulse is to shift the starting point of the spiral so that oscillations due to CTs occur on the whole duration of the second pulse. Assuming a sufficient time interval between the two pulses to avoid any overlap, the probability amplitude induced by the first pulse  $a_{e1}(t)$  has reached its asymptotic value  $a_{e1}(\infty)$  when the interaction with the second pulse starts. For a probe pulse significantly shorter than the details one wants to retrieve on the excited state population, the recorded fluorescence  $S^\theta(\tau)$  is directly proportional to the excited state population. During (or after) the second pulse, it can be written as

$$\begin{aligned} S^\theta(\tau) &= |a_{e1}(\infty) + e^{i\theta}a_{e2}(\tau)|^2 \\ &= |a_{e1}(\infty)|^2 + |a_{e2}(\tau)|^2 + 2 \operatorname{Re} [e^{i\theta}a_{e1}^*(\infty)a_{e2}(\tau)] \end{aligned} \quad (4)$$

$|a_{e1}(\infty)|^2$  can be deduced from a measurement of  $S^\theta(\tau)$  in the interval between the two exciting pulses. In order to determine the complex number associated to the probability amplitude, at least a second measurement is necessary as described in the next subsection.

## B. Reconstruction techniques

The probability amplitude produced by the second pulse  $E_{pu2}(t)$  is retrieved by combining the CTs scans  $S^\theta(\tau)$  (see Eq. 4) obtained for different values of the programmable phase

$\theta$ . The goal here is to extract the cross term  $a_{e_1}^*(\infty)a_{e_2}(\tau)$  from a set of scans. The factor  $a_{e_1}^*(\infty)$  is deduced - except for its phase - from the fluorescence observed at the end of the first pulse. We will show here different possible reconstruction schemes. As an example, we simulate the CTs corresponding to the following two-pulse sequence : the first pulse is 100 fs long, the second one is chirped to 10 ps ( $2 \cdot 10^5$  fs<sup>2</sup> quadratic phase) and delayed by 6 or 10 ps. Both pulses are resonant  $\omega_{pu} = \omega_{eg}$  and have the same energy. Determining the real and imaginary part of the probability amplitude requires at least two equations, which means two CT scans with different values of  $\theta$ . In this case, a system of two second order equations is obtained. A geometric method is used to solve it. With a third measurement, the quadratic term in Eq. 4 can be removed in order to obtain a linear system.

With a set of three scans, the angles  $\theta_k (k = 0, 2)$  must be chosen so that the corresponding matrix is not singular. This is the case for instance with  $\theta_k = 2k\pi/3$ . The corresponding CTs are plotted in Fig. 4. From these measurements, we calculate  $S^{[3]}(\tau)$  defined as :

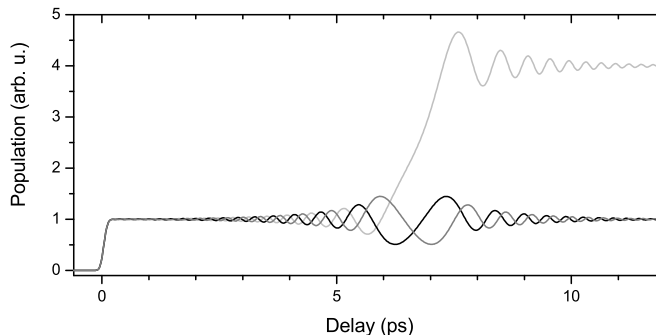


FIG. 4 – Theoretical CTs for a three-scans reconstruction : pulse sequence with  $\phi_{pu}^{(1)} = 6$  ps,  $\phi_{pu}^{(2)} = -2 \cdot 10^5$  fs<sup>2</sup> and  $\theta_k = 2k\pi/3$ .  $\theta_0 = 0$  : light grey line ;  $\theta_1 = 2\pi/3$  : black line ;  $\theta_2 = 4\pi/3$  : grey line.

$$S^{[3]}(\tau) = \frac{1}{3}S^0(\tau) - \frac{(1 + i\sqrt{3})}{6}S^{2\pi/3}(\tau) - \frac{(1 - i\sqrt{3})}{6}S^{4\pi/3}(\tau) = a_{e_1}^*(\infty)a_{e_2}(\tau) \quad (5)$$

Alternatively, the probability amplitude can be retrieved from a set of two CT measurements provided that a system of two nonlinear equations is solved. For two different values

of  $\theta$ , for example 0 and  $\alpha \neq 0, \pi$ , we thus have to solve the two-equation system :

$$S^0(\tau) = |a_{e1}(\infty)|^2 + |a_{e2}(\tau)|^2 + 2 \operatorname{Re} [a_{e1}^*(\infty)a_{e2}(\tau)] \quad (6a)$$

$$S^\alpha(\tau) = |a_{e1}(\infty)|^2 + |a_{e2}(\tau)|^2 + 2 \operatorname{Re} [e^{i\alpha} a_{e1}^*(\infty)a_{e2}(\tau)] \quad (6b)$$

If the second pulse is much weaker than the first one, the quadratic term in  $|a_{e2}(\tau)|$  can be neglected to obtain a simple linear equation system. In this case one easily obtains a unique solution and  $\alpha = \pi/2$  is the simplest choice.

Generally, the non-linear equation system gives two different solutions and only one is physically acceptable. To easily identify this solution and separate it from the other one, we have developed a geometric reconstruction which is described in detail in the appendix.

## IV. EXPERIMENT

### A. Experimental set-up

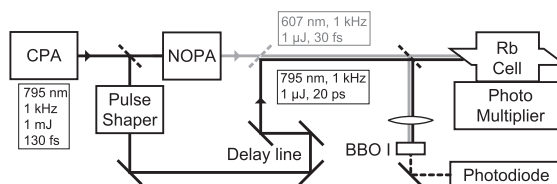


FIG. 5 – Experimental set-up. NOPA : non collinear optical parametric amplifier ; CPA : chirped pulse amplifier

The experimental set-up is displayed in Fig. 5. The  $5s - 5p$  ( $P_{1/2}$ ) transition (at 795 nm) is resonantly excited with a pulse sequence. The transient excited state population is probed "in real time" on the ( $5p - (8s, 6d)$ ) transitions with an ultrashort pulse (at 607 nm). The laser system is based on a conventional Ti : Sapphire laser with chirped pulse amplification (Spitfire Spectra Physics) which supplies 1 mJ -130 fs -795 nm pulses. Half of the beam is used for the pump pulse. The remaining seeds a home made Non-collinear Optical Parametric Amplifier (NOPA) compressed using double pass silica prisms, which delivers pulses of a few microJoule, 30 fs -FWHM pulse intensity, centered around 607 nm. The pump pulse is shaped with a programmable pulse-shaping device producing the pulse sequence, recombined with the probe pulse and sent into a sealed rubidium cell. The pump-probe signal is detected

by monitoring the fluorescence at 420 nm due to the radiative cascade (8s, 6d) - 6p - 5s collected by a photomultiplier tube as a function of the pump-probe delay. In parallel, a cross-correlation of the pump pulse sequence is recorded. The pulse shaping device is a 4f set-up composed of one pair each of reflective gratings and cylindrical mirrors. Its active elements -two 640 pixels liquid crystal masks- are installed in the common focal plane of both mirrors. This provides high resolution pulse shaping in phase and amplitude [17]. This is used to generate the shaped pump pulse sequence by applying the function

$$H^\theta(\omega) = \frac{1}{2}\mathbb{1} + \frac{1}{2} \exp \left[ i\theta + i\phi_{pu}^{(1)}(\omega - \omega_{pu}) + i\frac{\phi_{pu}^{(2)}}{2}(\omega - \omega_{pu})^2 \right] \quad (7)$$

The laser is centered at resonance ( $\omega_{pu} = \omega_{eg}$ ).

## B. Interferometric stability

The relative stability of the two pulse sequence is a crucial point in the present experiment. Both the relative phase and delay between the two pulses of the pump sequence should be kept stable as compared to  $2\pi$  or to the optical period  $T_o$ . Experiments of wave packet interferences have been performed with a Michelson interferometer used to produce the pulse pair. The delay was either actively [18, 19, 20] or passively [21, 22, 23, 24, 25] stabilized using different techniques. The best achieved stability is better than  $T_o/100$  with a Michelson placed under vacuum [25].

Alternatively, in experiments where only the amplitude of the interference pattern is needed, different strategies have been developed. These are based either on periodic modulation of the delay followed by a lock-in amplifier [26, 27], or random fluctuations applied to the delay followed by measurement of the resulting noise [28, 29, 30].

In our approach, the required stability and control of the phase and delay are naturally provided by the phase and amplitude pulse shaper [17]. As an illustration, we have performed demonstration experiments with a pump sequence consisting of two identical Fourier transform limited pulses, delayed by 3 ps. In a first example (see Fig. 6), the relative phase (at the resonance frequency) is set to 0 and  $\pi$  for two scans of the pump - probe delay. Two cross-correlations measurements (Fig. 6a and b) illustrate the relative position of the pulses. The phase shift of  $\pi$  does not affect these cross-correlations. In the pump-probe scan, the three positions of the probe pulse with respect to the pump sequence lead to : (i) No fluorescence

signal when the probe is before the pump pulses, (ii) a constant signal independent of the relative phase for the probe before the pump pulses, (iii) constructive ( $\theta = 0$ ) or destructive ( $\theta = \pi$ ) interferences for a probe pulse after the pump sequence. In the constructive interference case, the fluorescence signal is 4 times the signal obtained with a single pulse, as expected from usual interferences.

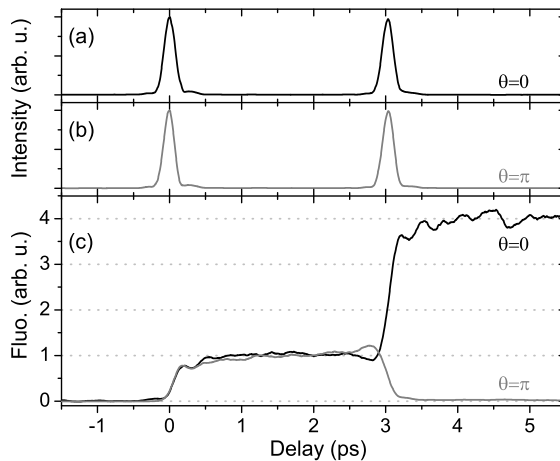


FIG. 6 – Experiments with a pump sequence of two Fourier Limited pulses centered at 795 nm and a 25 fs probe pulse at 607 nm, as a function of the probe pulse delay. Pump-probe cross-correlations for a relative phase of 0 (a) or  $\pi$  (b). (c) Fluorescence from the 8s-6d states for the two relative phases (black line :  $\theta = 0$ ; Gray line :  $\theta = \pi$ ).

In a second experiment, the pump-control delay is set to a constant value of 267 ps and the relative phase is scanned (Fig. 7). These two results illustrate both the excellent stability of the set-up and the control over the programmable phase.

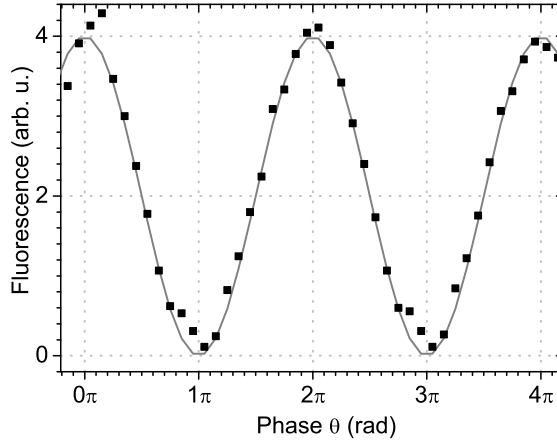


FIG. 7 – Same scheme as in Fig. 6 but with a fixed pump - probe delay and a variable relative phase. Experiment (Squares) and sine fit (solid grey line).

## V. RESULTS AND DISCUSSION

We present a series of results obtained with a sequence of two pulses generated by the high resolution phase and amplitude pulse shaper : The first one is close to Fourier limited (a replica of the input pulse) and the second one is time delayed ( $\phi_{pu}^{(1)} = 6$  ps) and strongly chirped ( $\phi_{pu}^{(2)} = -2.10^5$  fs<sup>2</sup>). Their amplitude are set equal. With phase and amplitude shaping, an extra relative phase  $\theta$  can easily be added to the second pulse. The various records correspond to different values of  $\theta$  and are used to illustrate the two reconstruction methods described in Section III B.

In the first example, three scans with phases separated by  $2\pi/3$  are used :  $\theta = \theta_0 + 2k\pi/3$  ( $k = 0, 1, 2$ ). The quality of the reconstruction does not depend on  $\theta_0$  and here we have  $\theta_0 \simeq 0.7$  (the reconstruction efficiency does not depend on  $\theta_0$ ). The scans are displayed in Fig. 8-a. As a difference to the case of a single chirped pulse (Fig. 2) [16], the three regimes are now clearly visible. The oscillations are observed before resonance as well as after resonance. The behavior during the passage through resonance depends directly on the relative phase  $\theta$ . A rapid increase, slow increase or slow decrease is observed resulting from constructive, partially constructive or destructive interferences. As expected, and similarly to the case of two FT limited pulses (see Fig. 6 and 7), the asymptotic value depends also strongly on  $\theta$ . The linear reconstruction method is used. The good stabilities of the laser and experimental set-up allow us using directly the raw data without any adjustment. The

excited state probability amplitude produced by the second pulse (with  $\theta = \theta_0$ ) is extracted from the three measurements and displayed in Fig.8-b). One observes clearly the expected Cornu spiral.

FIG. 8 – a) Experimental Coherent Transients resulting from the excitation of the atom by a FT limited pulse (at time  $\tau = 0$ ) followed by a chirped pulse ( $\phi_{pu}^{(1)} = 6$  ps,  $\phi_{pu}^{(2)} = -2.10^5$  fs<sup>2</sup>), for three different relative phases  $\theta_0 \simeq 0.7$  (light grey line),  $\theta = \theta_0 + 2\pi/3$  (black line) and  $\theta = \theta_0 + 4\pi/3$  (dark grey line) between the two pulses. b) Probability amplitude  $a_{e,2}(\tau)$  reconstructed from the three measurements presented in a), using a linear reconstruction and displayed in the complex plane. The Cornu spiral appears clearly.

In the second example displayed in Fig. 9, two scans with phases separated by  $\pi/2$  :  $\theta = \theta_0$  and  $\theta_0 + \pi/2$  are used for the nonlinear reconstruction. Here  $\theta_0 \simeq -0.8$ . The nonlinear method requires determining separately the population  $|a_{e1}(\infty)|^2$  created by the first pulse. The plateau immediately after the end of the first pulse is used for this purpose. The excited state probability amplitude produced by the second pulse and extracted from the two measurements is displayed in Fig. 9b. The reconstructed probability amplitude is also displayed in Fig. 10 in a 3D plot (real and imaginary part of the probability amplitude as a function of time). The projections on the various 2D planes are also displayed. The expected Cornu spiral [16] is clearly seen in the complex plane.

In previous experiments [12, 16], only the excited state probability was measured. Here, the initial preparation of a coherent superposition of  $|e\rangle$  and  $|g\rangle$  by the first pulse allowed measuring the probability amplitude in real time during its evolution in interaction with the

FIG. 9 – a) Experimental Coherent Transients resulting from the excitation of the atom by a FT limited pulse (at time  $\tau = 0$ ) followed by a chirped pulse ( $\phi_{pu}^{(1)} = 6$  ps,  $\phi_{pu}^{(2)} = -2.10^5$  fs<sup>2</sup>), for two different relative phases  $\theta_0 \simeq -0.8$ ,  $\theta = \theta_0 + \pi/2$  between the two pulses. b) Probability amplitude  $a_{e,2}(\tau)$  reconstructed from the two measurements presented in a) and displayed in the complex plane. The Cornu spiral appears clearly.

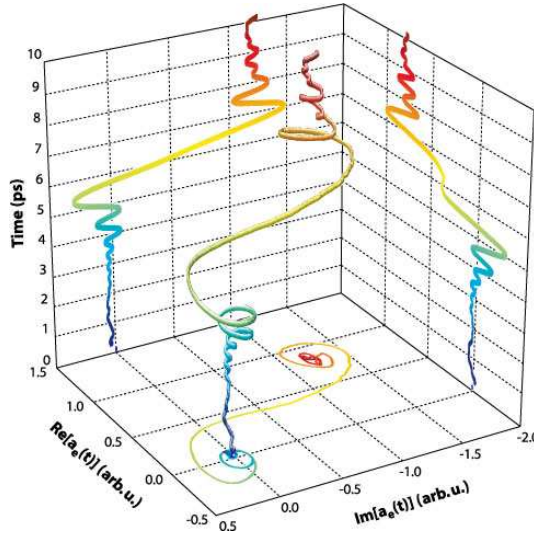


FIG. 10 – 3D spiral representing the time evolution of the excited state probability amplitude (same data as in Fig. 9). The vertical axis represents the time.

laser pulse.

The two methods provide similar quality of reconstruction. The linear approach requires three measurements. It increases the recording time by a factor of 1.5 as compared to the nonlinear method. Conversely it is more robust and can be used in a wider variety of situations (relative phase, intensity ...). A larger number of recordings could be combined in a linear square fit approach to improve the accuracy of the measurement. This would of course be at the extent of the recording time.

Several examples of quantum phase measurements of states created by ultrashort pulses are based on interferences between an unknown wave function and a "reference" wave function. These wave functions are created by a sequence of two ultrashort pulses (an unknown pulse and a reference pulse). The quantum state created by the unknown pulse is deduced either by time- and frequency- integrated fluorescence measured as a function of the delay [31], or by measuring the population of each eigenstate for different values of the relative phases [32]. Alternatively, the amplitude of noise resulting from random fluctuations of the delay is measured [30, 33]. In another approach, the dispersed fluorescence emitted by an oscillating nuclear wave packet in a diatomic molecule was recorded as a function of time [34]. In this case, the fluorescence wavelength - position relationship is derived from the Franck-Condon principle.

In all these examples involving several excited states, either a particular selectivity is used to detect independently each excited state, or the delay is used to obtain a set of measurements which are then inverted to obtain the amplitude of each quantum state. In our study, only one single excited state is involved and the measurements are performed at the same delay. This ensures determining the temporal evolution of the quantum state.

Our quantum state measurement method can be extended to the case of  $p$  excited states  $(|i\rangle)_{i=1,p}$  of different energies  $\hbar\omega_i$ . Their probability amplitudes can be retrieved from a set of  $2p+1$  measurements in a linear reconstruction scheme. As an example, the first measurement can be performed with the second pulse  $E_{pu_2}(t)$  only, providing

$$S^\emptyset(\tau) = \sum_{i=1}^p |a_{i2}(\tau)|^2 \quad (8)$$

This allows thus to remove the nonlinear contributions from the subsequent measurements. The remaining  $2p$  measurements are performed with the two pulse sequence, each with a set of  $p$  phases  $(\theta_{i,k})_{i=1,p}$  for  $k = 1, 2p$  applied at the frequencies  $\omega_i$ . They provide with the quantity

$$S_k(\tau) = \sum_{i=1}^p |a_{i1}(\infty)|^2 + \sum_{i=1}^p |a_{i2}(\tau)|^2 + 2 \sum_{i=1}^p \text{Re} [e^{i\theta_{i,k}} a_{i1}^*(\infty) a_{i2}(\tau)] \quad (9)$$

As in the case with a single excited pulse,  $\sum_{i=1}^p |a_{i1}(\infty)|^2$  can be deduced from a measurement of  $S_k(\tau)$  in the interval between the two exciting pulses. Since the phases can be chosen independently, it is always possible to find a set of phases for which the system of  $2p$  lin-

ear equations can be inverted. This would not be the case if the phases were not applied independently but through an extra delay  $\tau'_k$  (giving  $\theta_{i,k} = \omega_{ig}\tau'_k$ ).

## VI. CONCLUSION

We have presented a new method to determine the real time evolution of an excited quantum state in interaction with an ultrashort laser pulse.

By simple derivation of the excited state probability amplitude, it is possible to retrieve the electric field (phase and amplitude) of the second pump pulse  $E_{pu_2}(t)$ , provided that the probe pulse is well known or short enough. The possibilities offered by this technique are discussed in detail elsewhere [14]. It can also be used for a differential measurement to analyze the changes induced by inserting a material. In this last case, the requirements on the properties of the probe pulse are less severe.

We thank Chris Meier for fruitful discussions.

## VII. APPENDIX

We detail here the geometrical reconstruction used to solve the set of second-order non-linear equations. This latter interprets the equation system (6) in terms of circles intersection in the complex plane. Figure 3 (a) shows the two CTs scans for  $\theta = 0$  (black) and  $\theta = \alpha$  (gray) used for the reconstruction (in the simulations  $\alpha = \pi/3$ ). The corresponding probability amplitudes are plotted in Fig. 3 (b). In both cases, the contribution of the first Fourier-limited pulse is a straight line and the contribution of the second pulse is a Cornu spiral. The phase  $\theta$  only changes the relative orientation of the line and the spiral. At any time  $\tau$ , the CTs values  $S^0(\tau)$  and  $S^\alpha(\tau)$  respectively correspond to  $r_0^2(\tau)$  and  $r_\alpha^2(\tau)$ , where  $r_0(\tau)$  and  $r_\alpha(\tau)$  are the distances in the complex plane between the origin and the current positions on both spirals (see Fig. 3 (b)). Retrieving the probability amplitude produced by the second pulse corresponds to geometrically reconstructing the black Cornu Spiral in Fig. 3 (b), using the two time dependant distances  $r_0(\tau)$  and  $r_\alpha(\tau)$ .

To achieve this, we mentally rotate the gray path by an angle of  $-\alpha$ , around the starting point of the Cornu Spiral (1,0). We then choose this point as the new origin for the complex plane. These transformations preserve both angles and distances and therefore do not change

our equation system. Figure 11 shows the two paths after the transformations. We call  $P_0$  and  $P_\alpha$  the starting points of each path whose coordinates are known :  $(-1,0)$  and  $(-\cos(\alpha), \sin(\alpha))$  respectively. Thanks to these transformations, the two Cornu Spirals are now superimposed and correspond to the amplitude probability we want to retrieve. The two distances  $r_0(\tau)$  and  $r_\alpha(\tau)$  can now be seen as the distances between the point  $a_{e_2}(\tau)$  on the Cornu spiral and two reference points  $P_0$  and  $P_\alpha$ . To geometrically reconstruct  $a_{e_2}(\tau)$

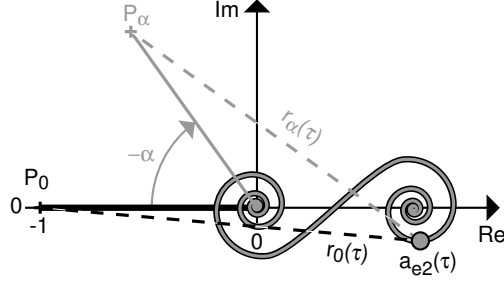


FIG. 11 – New geometric interpretation :  $r_0(\tau)$  and  $r_\alpha(\tau)$  are the distances between  $a_{e_2}(\tau)$  and two reference points  $P_0$  et  $P_\alpha$ .

one just needs to find, for every time  $\tau$ , the intersection of the circle  $\mathcal{C}_0$  (centered on  $P_0$  with a radius  $r_0(\tau)$ ) and the circle  $\mathcal{C}_\alpha$  (centered on  $P_\alpha$  with a radius  $r_\alpha(\tau)$ ), as depicted in figure 12. We get two different solutions,  $a_{e_2}^+(\tau)$  and  $a_{e_2}^-(\tau)$ . The physically acceptable one

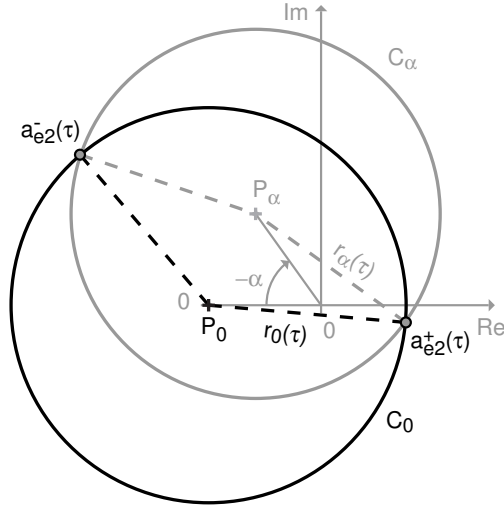


FIG. 12 – Geometric reconstruction of  $a_{e_2}(\tau)$ . Two solutions  $a_{e_2}^+(\tau)$  and  $a_{e_2}^-(\tau)$  are available ; The physical one starts in  $(0,0)$ .

starts in  $(0,0)$ . To avoid degeneracy, the Cornu spiral should not cross the  $(P_0, P_\alpha)$  line.

Two ways of pushing the spiral away from  $(P_0, P_\alpha)$  are increasing the intensity of the first pulse, and reducing the angle  $\alpha$ . However, a too small angle leads to near-degeneracy of the circles, increasing thus the uncertainties in determining their crossing points. Usually, the reconstruction works well with a first pulse at least as intense as the second one and an angle  $\alpha$  in the interval  $[\pi/4, \pi/2]$ .

- 
- [1] M. A. Bouchene, V. Blanchet, C. Nicole, N. Melikechi, B. Girard, H. Ruppe, S. Rutz, E. Schreiber, and L. Wste, “Temporal coherent control induced by wave packet interferences in one and two photon atomic transitions,” *Eur. Phys. J. D* **2**(2), 131 (1998).
- [2] R. R. Jones, D. W. Schumacher, T. F. Gallagher, and P. H. Bucksbaum, “Bound-state interferometry using incoherent light,” *J. Phys. B* **28**(13), L405 (1995).
- [3] R. S. Judson and H. Rabitz, “Teaching lasers to control molecules,” *Physical Review Letters* **68**(10), 1500–3 (1992).
- [4] W. S. Warren, H. Rabitz, and M. Dahleh, “Coherent Control of Quantum Dynamics : The Dream is Alive,” *Science* **259**, 1581 (1993).
- [5] A. Assion, T. Baumert, M. Bergt, T. Brixner, B. Kiefer, V. Seyfried, M. Strehle, and G. Gerber, “Control of Chemical Reactions by Feedback-optimized Phase-shaped femtosecond laser pulses,” *Science* **282**, 919 (1998).
- [6] R. J. Levis, G. M. Menkir, and H. Rabitz, “Selective Bond Dissociation and Rearrangement with Optimally Tailored, Strong-Field Laser Pulses,” *Science* **292**(5517), 709–713 (2001).
- [7] J. L. Herek, W. Wohlleben, R. J. Cogdell, D. Zeidler, and M. Motzkus, “Quantum control of energy flow in light harvesting,” *Nature* **417**(6888), 533 (2002).
- [8] C. Daniel, J. Full, L. Gonzalez, C. Lupulescu, J. Manz, A. Merli, S. Vajda, and L. Wöste, “Deciphering the reaction dynamics underlying optimal control laser fields,” *Science* **299**(5606), 536–539 (2003).
- [9] D. Meshulach and Y. Silberberg, “Coherent Quantum Control of 2-Photon Transitions by a Femtosecond Laser-Pulse,” *Nature* **396**(6708), 239–242 (1998).
- [10] H. U. Stauffer, J. B. Ballard, Z. Amitay, and S. R. Leone, “Simultaneous phase control of  $Li_2$  wave packets in two electronic states.” *J. Chem. Phys.* **116**(3), 946 (2002).

- [11] N. Dudovich, D. Oron, and Y. Silberberg, “Coherent transient enhancement of optically induced resonant transitions,” *Physical Review Letters* **88**(12), 123,004–1–4 (2002).
- [12] J. Degert, W. Wohlleben, B. Chatel, M. Motzkus, and B. Girard, “Realization of a Time-Domain Fresnel Lens with Coherent Control,” *Physical Review Letters* **89**(20), 203,003 (2002).
- [13] W. Wohlleben, J. Degert, A. Monmayrant, B. Chatel, M. Motzkus, and B. Girard, “Coherent transients as a highly sensitive probe for femtosecond pulse shaper,” *Applied Physics B (Lasers and Optics)* **79**(4), 435 – 439 (2004).
- [14] A. Monmayrant, B. Chatel, and B. Girard, “Femtosecond pulse shape reconstruction from coherent transient measurements,” *Optics Letters* **in press** (2005).
- [15] A. Monmayrant, B. Chatel, and B. Girard, “Atomic spirograph : measurement of the excited state wave function using coherent transients,” *Physical Review Letters* **submitted** (2005).
- [16] S. Zamith, J. Degert, S. Stock, B. de Beauvoir, V. Blanchet, M. A. Bouchene, and B. Girard, “Observation of Coherent Transients in Ultrashort Chirped Excitation of an undamped Two-Level System,” *Physical Review Letters* **87**(3), 033,001 (2001).
- [17] A. Monmayrant and B. Chatel, “A new phase and amplitude high resolution pulse shaper,” *Review of Scientific Instruments* **75**(8), 2668–71 (2004).
- [18] N. F. Scherer, A. J. Ruggiero, M. Du, and G. R. Fleming, “Time resolved dynamics of isolated molecular systems studied with phase-locked femtosecond pulse pairs,” *J. Chem. Phys.* **93**(1), 856 (1990).
- [19] N. F. Scherer, R. J. Carlson, A. Matro, M. Du, A. J. Ruggiero, V. Romerorochin, J. A. Cina, G. R. Fleming, and S. A. Rice, “Fluorescence-Detected Wave Packet Interferometry - Time Resolved Molecular Spectroscopy with Sequences of Femtosecond Phase-Locked Pulses,” *J. Chem. Phys.* **95**(3), 1487 (1991).
- [20] N. Belabas, J. P. Likforman, L. Canioni, B. Bousquet, and M. Joffre, “Coherent broadband pulse shaping in the mid infrared,” *Optics Letters* **26**(10), 743–5 (2001).
- [21] R. R. Jones, C. S. Raman, D. W. Schumacher, and P. H. Bucksbaum, “Ramsey interference in strongly driven Rydberg systems,” *Phys. Rev. Lett.* **71**(16), 2575 (1993).
- [22] V. Blanchet, M. A. Bouchene, O. Cabrol, and B. Girard, “One Color Coherent Control in Cs2 : Observation of 2.7 fs Beats in the Ionization Signal,” *Chem. Phys. Lett.* **233**, 491 (1995).

- [23] V. Blanchet, C. Nicole, M. A. Bouchene, and B. Girard, “Temporal coherent control in two-photon transitions : from optical interferences to quantum interferences,” *Phys. Rev. Lett.* **78**(14), 2716 (1997).
- [24] V. Blanchet, M. A. Bouchene, and B. Girard, “Temporal coherent control in the photoionization of Cs2 : Theory and Experiment,” *J. Chem. Phys.* **108**(12), 4862 (1998).
- [25] K. Ohmori, Y. Sato, E. E. Nikitin, and S. A. Rice, “High-Precision Molecular Wave-Packet Interferometry with HgAr Dimers,” *Phys. Rev. Lett.* **91**(24), 243,003 (2003).
- [26] B. Broers, J. Christian, J. Hoogenaard, W. van der Zande, H. van Linden van den Heuvell, and L. Noordam, “Time-resolved dynamics of electronic wave packets above the classical field-ionisation threshold.” *Phys. Rev. Lett.* **71**(3), 344 (1993).
- [27] N. A. Papadogiannis, B. Witzel, C. Kalpouzos, and D. Charalambidis, “Observation of Attosecond Light Localization in Higher Order Harmonic Generation,” *Phys. Rev. Lett.* **83**, 4289 (1999).
- [28] O. Kinrot, I. Averbukh, and Y. Prior, “Measuring Coherence while Observing Noise.” *Phys. Rev. Lett.* **75**(21), 3822 (1995).
- [29] C. Leichtle, W. P. Schleich, I. S. Averbukh, and M. Shapiro, “Wave packet interferometry without phase-locking,” *J. Chem. Phys.* **108**(15), 6057 (1998).
- [30] T. C. Weinacht, J. Ahn, and P. H. Bucksbaum, “Measurement of the Amplitude and Phase of a Sculpted Rydberg Wave Packet,” *Phys. Rev. Lett.* **80**(25), 5508 (1998).
- [31] C. Leichtle, W. P. Schleich, I. S. Averbukh, and M. Shapiro, “Quantum State Holography,” *Physical Review Letters* **80**(7), 1418–21 (1998).
- [32] X. Chen and J. A. Yeazell, “Reconstruction of engineered atomic wave functions via phase-dependent population measurements,” *Phys. Rev. A* **56**(3), 2316 (1997).
- [33] T. C. Weinacht, J. Ahn, and P. H. Bucksbaum, “Controlling the shape of a quantum wavefunction,” *Nature* **397**, 233 (1999).
- [34] V. Wong and I. A. Walmsley, “Linear filter analysis of methods for ultrashort pulse shape measurements,” *J Opt Soc Am B Opt Physics* **12**, 1491 (1995).